On the Distributed Coupled-Line Digital Frequency Multipliers -Part ?: Output Simulations to Cosine Half Wave Inputs

On the Distributed Coupled-Line Digital Frequency Multipliers-Part II : Output Simulations to Cosine Half Wave Inputs

Iwata SAKAGAMI

Abstract

The simulations of output responses of distributed coupled-line digital frequency multipliers are discussed. The simulated waveforms are obtained from sampled data of measured amplitude and phase characteristics and found to be in good agreement with experimental photographs.

The input signals here are the cosine half wave pulses sliced at a positive level. Therefore the Fourier transform and the energy ratio within a specified frequency band are also considered.

1. Introduction

Speeding up a train of unipolar or bipolar pulses without using nonlinear elements has been discussed for the case of distributed coupled-line (briefly, DCL) networks [1, 2]. The main theme of these past papers was how to synthesize DCL networks from network transfer functions and impulse responses. For the network synthesis, it has been convenient to treat a train of input pulses as a train of impulses. The reasons were as follows: (i) The train of input impulses possesses equi-amplitude and equi-spacing discrete frequency components over $-\infty < f < \infty$ [3], and (ii) the frequency and phase characteristics of the DCL networks are also periodical at all frequencies of $-\infty < f < \infty$, as the network transfer functions are expressed by the delay operator $z^{-1} = \exp(-2s\tau)$ or the Richards variable $t = j\tan \beta \ell$ [See II. in [2] for the symbols τ, β, ℓ, and s]. Theoretically, the property of (i) can be matched to that of (ii) at all frequencies, and this eases the synthesis problems.

Normally, the transfer functions of DCL networks are calculated on the basis of TEM wave approximations. Arbitrary waveforms are allowable as input pulses if the waveforms are duration-limited and no overlap occurs at the output port. However, a train of cosine half wave (CHW) pulses will be introduced in this paper for the reasons that (i) the CHW pulse occupies the narrowest bandwidth among many other duration-limited waveforms [4], (ii) the train of CHW pulses can be obtained easily from a sinusoidal oscillator, and (iii) the train of CHW pulses is considered to be suitable to the high speed pulse transmissions.

The main topics here are: (i) A CHW pulse in more general form [See Fig. 1] and the Fourier transform; (ii) Energy within a specified frequency; (iii) Energy spectra of periodical CHW pulses; and (iv) Simulations of output responses of the DCL digital frequency multipliers.

In this way, the functions of the digital frequency multipliers will be clarified and verified from the considerations of these subjects.

2. Energy Ratio of a CHW Pules on the Frequency Axis

A. Fourier Transform and Effective Bandwidth

Fig. 1 shows a cosine half wave (CHW) pulse which is sliced at a positive voltage level from a sinusoidal wave. The waveform v (t) is

$$v(t) = \begin{cases} A(\cos\omega_0 t - \cos\theta_0), & |t| \leq aW \\ 0, & |t| > aW \end{cases} \qquad (1)$$

where, $\omega_0 = \pi / 2W$, $\theta_0 = a\pi / 2$, and $0 < a \leq 1$.

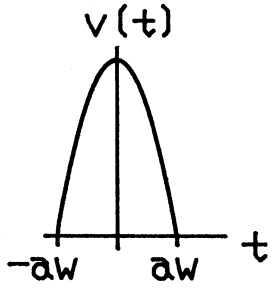

Fig. 1 A cosine half wave (CHW) pulse ($0 < a \leq 1$).

The a is variable and represents the positive voltage slice level indirectly. The 2W indicates the duration of the CHW pulse at = 1. Designating the Fourier transform of v(t) by $V(\omega)$, the CHW pulse sliced at zero voltage level is given by a = 1 and represented by

$$v(t) = \begin{cases} \frac{1}{\sqrt{W}} \cos(\omega_0 t), & |t| \leq W \\ 0 & |t| \leq W \end{cases} \qquad (2a)$$

$$V(\omega) = \begin{cases} 4\pi\sqrt{W}\cos(W\omega) / (\pi^2 - 4W^2\omega^2), & \omega \neq \pm\pi / 2W \\ \sqrt{W}, & \omega = \pm\pi / 2W \end{cases} \qquad (2b)$$

(1) needs to be discussed at first for the following reasons: In general, CHW pulses created by diode circuits and so forth correspond to the case of $0 < a < 1$; and a train of CHW pulses with variable duty ratio can be obtained from a sinusoidal oscillator by changing the positive slice level, though this is a rather primitive method.

For the waveform of total energy 1,

$$\int_{-\infty}^{\infty} |v(t)|^2 dt = \frac{1}{2\pi} \int_{-\infty}^{\infty} |v(\omega)|^2 d\omega = 1 \qquad (3)$$

Using (3), A in (1) can be given by

$$A = \sqrt{\pi} \,/\, \sqrt{W\{\, 2a\pi + a\pi\cos(a\pi) - 3\sin(a\pi)\,\}} \tag{4}$$

By (A. 2) defined in the Appendix, the effective bandwidth $\Delta\omega$ of (1) is rewritten by

$$(\Delta\omega)^2 = \int_{-aW}^{aW} |dv(t)/dt|^2 \, dt. \tag{5}$$

Calculating (5),

$$\Delta\omega = \frac{\pi}{2W}\sqrt{\frac{a\pi - \sin(a\pi)}{2a\pi + a\pi\cos(a\pi) - 3\sin(a\pi)}} \tag{6}$$

$V(\omega)$ can be given by

$$V(\omega) = 4W\pi AP(X), \tag{7}$$

where

$$P(X) = \frac{X\sin(\theta_0)\cos(X/2) - a\pi\cos(\theta_0)\sin(X/2)}{X(\pi + X/a)(\pi - X/a)} \tag{7a}$$

$$X = 2aW\omega. \tag{7b}$$

Putting

$$\tau_1 = 2aW, \tag{8}$$

τ_1 denotes the pulse duration in Fig. 1.

Eqs. (1) and (4) in case of $a = 1$ represent the same equation as in (2a). In the same way, (7) becomes equal to (2b).

B. Energy within $|\omega| \leq \Omega$

As the total energy of v (t) is 1 due to (3) and (4), the energy ratio E_{ra} of the energy included within $|\omega| \leq \Omega$ to the total energy is given by

$$E_{ra} = \frac{1}{2\pi}\int_{-\Omega}^{\Omega} |v(\omega)|^2 \, d\omega \tag{9a}$$

$$= \frac{4W\pi A^2}{a}\int_{-\tau_1\Omega}^{\tau_1\Omega} |P(X)|^2 \, dX. \tag{9b}$$

P (X) at $X = O, \pm a\pi$ are given by

$$\lim_{X\to O} P(X) = \frac{2\sin(\theta_0) - a\pi\cos(\theta_0)}{2\pi^2}, \tag{10a}$$

$$\lim_{X\to \pm a\pi} P(X) = \frac{a\pi - \sin(a\pi)}{4\pi^2}. \tag{10b}$$

Taking (10) into account, the numerical calculations of E_{ra} are carried out as a function of $(\tau_1\Omega)$

by the double precision Romberg method. The results are shown in Fig. 2. The curves Co. 1 and Co. 2 represent cases of a = 1 and a = 0. 5, respectively. The curve of Rec. indicates the energy ratio of a rectangular wave [See (A. 5) in appendix], presented for comparison with the CHW pulses. It is known that the effective bandwidth $\Delta\omega$ of the CHW pulse of a = 1 is the narrowest among many other duration limited pulses [See (A. 4) ; when $\tau_1 = 2W$, (A.4) is equal to (2a).]. However, there are no practical differences between Co. 1 and Co. 2, so that the case of energy ratio 99% is examined numerically at first as a standard of bandwidth required for the network design.

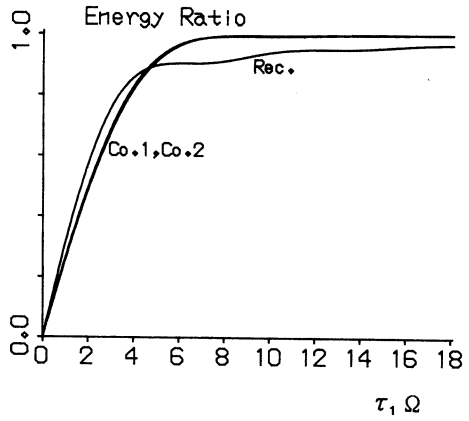

Fig. 2 The energy ratio within $|\omega| \leq \Omega$ as a function of $(\Omega\tau_1)$.

(i) The case of $E_{ra} = 0.99$

When a = 1, we have $\tau_1\Omega = 7.426$. For the pulse duration $\tau_1 = 1.1$ nsec [See C., V. in [2]], we have $f_\Omega = 1.074$ GHz. Here $f_\Omega = \Omega / 2\pi$. When a = 0.5, we have $\tau_1\Omega = 7.484$. This means $f_\Omega = 1.083$ GHz for the same value of τ_1.

The f_Ω of this case indicates that 99% energy of a CHW pulse is included within $|f| \leq f_\Omega$.

(ii)The case of $E_{ra} = 0.997$

It is known that the energy ratio of a Gaussian pulse exceeds 99.7% at three times the effective bandwidth of the Gaussin pulse. For the confirmation, the case of $E_{ra} = 0.997$ is also examined about the CHW pulses. For a = 1.0, and 0.5, we have $\tau_1\Omega = 12.11$, and 12.60. Using (6), we have $\Omega / \Delta\omega = 3.85$, and 4.0, respectively. This means the energy of 99.7% of the CHW pulses of a = 1 and a = 0.5 are included within 3.85 times and 4.0 times $\Delta\omega$.

(iii) The case of rectangular pulse

In order to exceed 99% energy, there must be $\tau_1\Omega \geq 64.63$. Therefore, a fairly large f_Ω is required.

In the following sections, the CHW pulse of a = 1 will be used for the calculation of output responses as the curves Co. 1 and Co. 2 are very close to each other.

3. Energy Spectrum of a Train of Input Pulses

Now let us consider a train of unipolar pulses $v_{Tr}(t)$ of time interval T (period T) and a train of bipolar pulses $w_{Tr}(t)$ of time interval T (period 2T) [For instance, see Figs. 6(a), (b)].

A. The Case of $v_{Tr}(t)$

The pulse train $v_{Tr}(t)$ and its Fourier transform are given by

$$v_{Tr}(t) = \frac{1}{T} \sum_{k=-\infty}^{\infty} V(k\omega^+) \exp(jk\omega^+ t), \qquad (-\infty < t < \infty) \tag{11a}$$

$$F[v_{Tr}(t)] = \omega^+ \sum_{k=-\infty}^{\infty} V(k\omega^+)\, \delta(\omega - k\omega^+), \tag{11b}$$

where $\omega^+ = 2\pi / T$. When the DCL n-section networks in Fig. 4 in [2] are used, $T = 2(n+1)\tau$. The τ indicates the time delay of a unit element [See Fig. 3 in [2]].

As the energy within a period is given by

$$\int_{-T/2}^{T/2} |v_{Tr}(t)|^2 dt = 1,$$

we have

$$\frac{1}{T} \sum_{k=-\infty}^{\infty} V^2(k\omega^+) = 1, \tag{12}$$

where $V(k\omega^+) = 4W\pi AP(X_k)$ and $X_k = k\omega^+ \tau_1$.

B. The Case of $w_{Tr}(t)$

The pulse train $w_{Tr}(t)$ and its Fourier transform are

$$w_{Tr}(t) = \frac{1}{T} \sum_{k=-\infty}^{\infty} V\{(2k+1)\omega^+/2\} \exp\{j(2k+1)\omega^+ t/2\}, \quad (-\infty < t < \infty) \tag{13a}$$

$$F[w_{Tr}(t)] = \omega^+ \sum_{k=-\infty}^{\infty} V\{(2k+1)\omega^+/2\}\, \delta\{\omega - (2k+1)\omega^+/2\}. \tag{13b}$$

The $w_{Tr}(t)$ alternates between the positive and negative polarities at time interval T. Assuming a positive polarity pulse arrives at the input port of the DCL networks at $t = 0$,

$$\int_{-T/2}^{T/2} |w_{Tr}(t)|^2 dt = 1,$$

Therefore, we have

$$\frac{1}{T} \sum_{k=-\infty}^{\infty} V^2\{(2k+1)\omega^+/2\} = 1, \tag{14}$$

where $V\{(2k+1)\omega^+/2\} = 4W\pi AP(X_k)$ and $X_k = (2k+1)\omega^+ \tau_1 / 2$.

From (11b) and (13b), it is understood that the frequency components of periodical unipolar pulses or those of bipolar pulses are discrete and given by integral multiples of ω^+ or odd number multiples of $\omega^+/2$ and the amplitudes are determined by the Fourier transform of each con-

stituent pulse. As (12) and (14) can be obtained by multiplying the mean power of periodical waves by the period, each term of the left side of each equation represents the energy spectrum.

C. Frequency Characteristics of Test Circuits A and B

Fig.3 shows the same measurement system as in Fig. 1 (a) in [2]. The design parameters of test circuits are the same as those in [2]. Therefore, the amplitude and phase characteristics can be

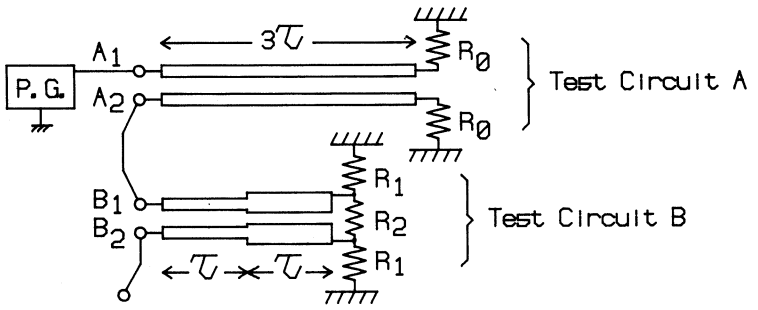

Fig. 3 Test circuits for measurement, where P. G., test circuit A and test circuit B indicate a pulse generator, a 1-section directional coupler and a 2-section coupled-line network.

calculated from their network transfer functions. Figs. 4 (a) and (b) show the amplitude and phase characteristics of test circuit A, and Figs. 5 (a) and (b) are those of test circuit B. In these figures, the theoretical curves are depicted by broken lines to suit the computer drawing. The equipment for the measurement was a set of HP8620A, HP8410A, HP8746B and HP8413A. For the amplitude characteristics, the measurement data were tied with solid lines directly. However, for the phase characteristics, there were not many measurement points. As seen from Fig. 4 (b), the theoretical curves have double values of $-90°$ and $+90°$ at integral multiples of 385MHz, so that the data from close to these transition points could not be measured accurately. Therefore, on the phase characteristics of Fig. 4 (b), the 3-rd order least mean square (LMS) polynomials $y = a_0 + a_1 x + a_2 x^2 + a_3 x^3$ were derived from the measurement data. In Fig. 5 (b), the situations are similr to the above.

D. Discrete Frequency Components of Input CHW Pulses

The trains of CHW pulses for the use of output simulations are respectively shown in Fig. 6 (a) and (b). In Fig. 6 (a), the period T_1 is 5. 2nsec and the duration of a CHW pulse τ_1 is 1.1nsec. In Fig. 6 (b), the pulse interval T_2 is $T_1 / 2$ or 2.6nsec and the duration is the same as in Fig. 6 (a).

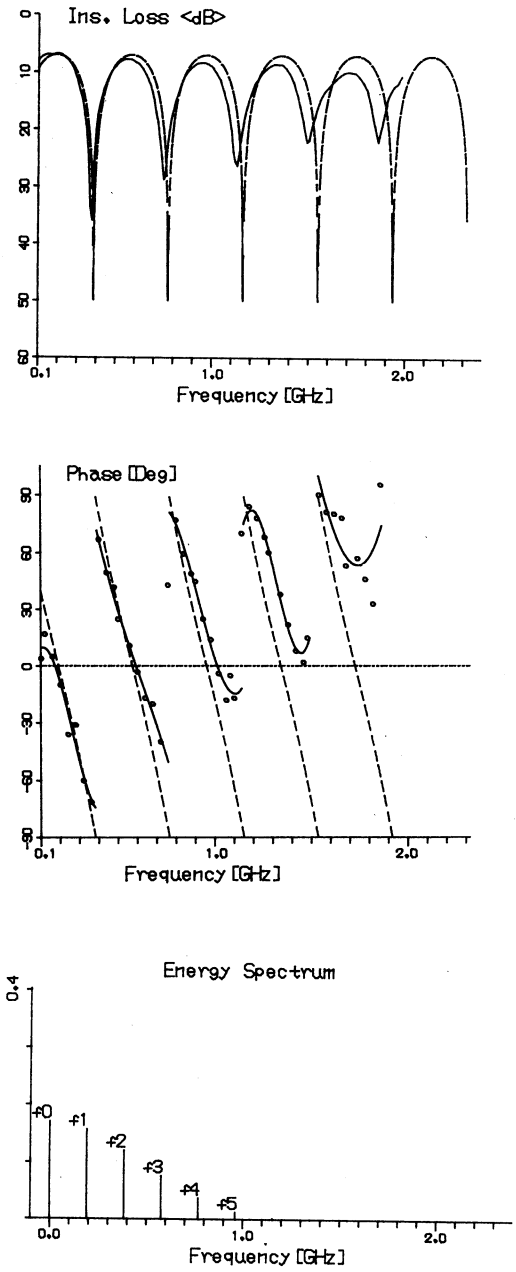

Fig. 4 (a)Amplitude characteristics of test circuit A. Solid lines: measured. Broken lines: theoretical.
(b)Phase characteristics of test circuit A.
⁓ : 3-rd order least mean square (LMS) polynomials.
Broken lines: theoretical.
(c)Energy spectra of Fig. 6 (a).

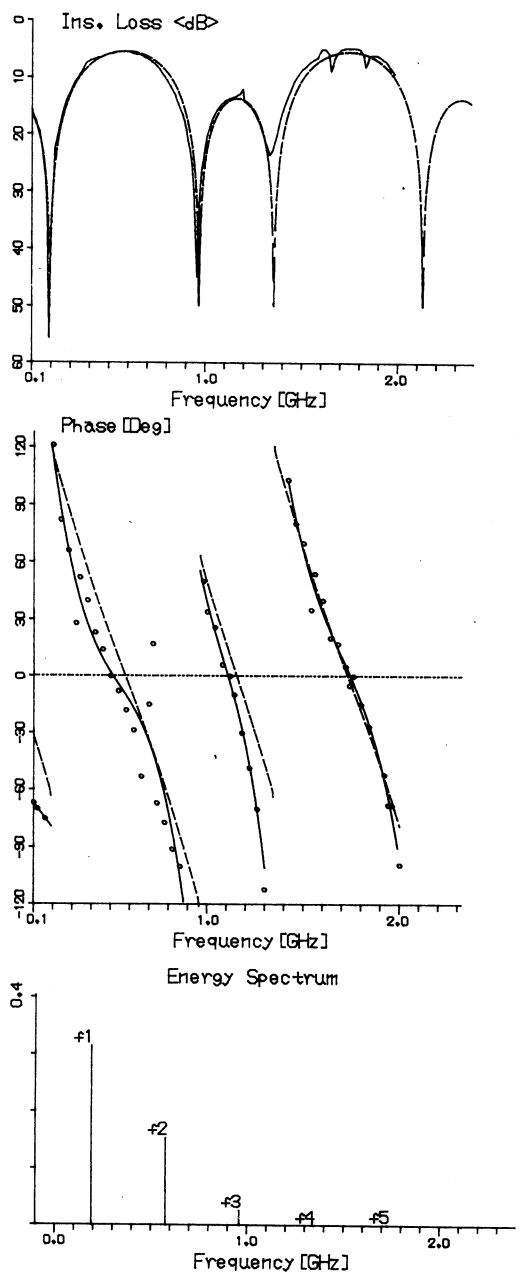

Fig. 5 (a)Amplitude characteristics of test circuit B. Solid lines: measured. Broken lines: theoretical.
(b)Phase characteristics of test circuit B
⁓ : 1-st order LMS polynomial for the first peried and 3-rd order LMS polynomials for other periods.
Broken lines: theoretical.
(c)Energy spectra of Fig. 6 (b).

Assuming that the pulse generator P. G. in Fig. 3 outputs the pulse train in Fig. 6 (a), the energy spectra calculated from (12) are shown in Fig. 4 (c). Similarly, assuming the test circuit A generates the pulse train in Fig. 6 (b), the energy spectra given in Fig. 5 (c) can be calculated from (14).

In Fig. 4 (c), the energy of the unipolar CHW pulse train exceeds 99% at f = 1.154 GHz, and the energy of 99.5% is included within $|f| \leq 1.154$GHz.
Within $|f| \leq 1.731$ GHz, the energy of 99.77% is included.

In Fig. 5 (c), the energy of the bipolar CHW pulse train exceeds 99% at f = 0.962GHz. The energy of 99.5% and that of 99.85% are respectively included for $|f| \leq 0.962$GHz and for $|f| \leq 1.731$GHz.

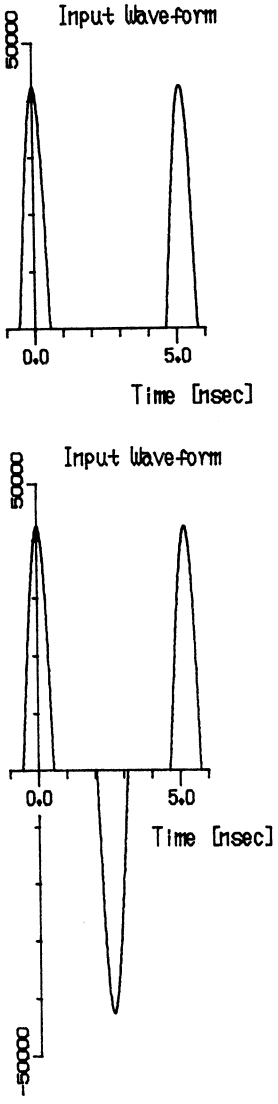

Fig. 6 Trains of CHW pulses.
(a) Input for test circuit A.
(b) Input for test circuit B.

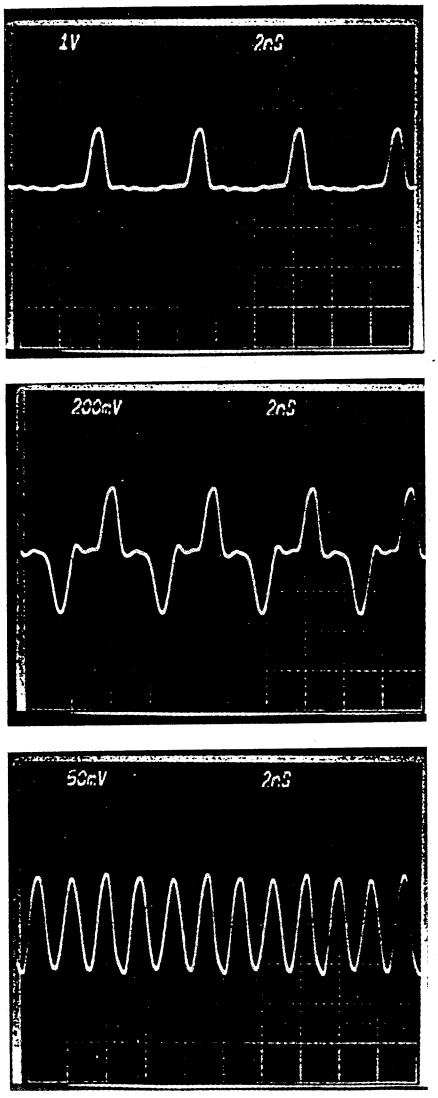

Fig. 7 Experimental results at
(a) port A_1, (b) port A_2, and
(c) port B_2.

In this paper, the measured data from zero to 1.731GHz are used for the output simulations.

The DC component f_0 in Fig. 4 (c) is cut off completely, as seen from the test circuit A. From Figs. 4 (a), (b) and (c), it is understandable why the frequency components f2, f4, ··· are rejected, and others f1, f3, ··· transmit to output port A_2. This is the reason why the output pulses can be

formed twice as fast as input. The test circuit A satisfies the prescribed amplitude and phase characteristics approximately in the region where almost all the energy of input pulse train is concentrated.

As seen from Fig. 5 (c), there is no DC component in the train of bipolar pulses. In Figs. 5 (a), (b) and (c), similarly to the case of Figs. 4 (a) (b) (c), the components f1, f3, f4, ··· are rejected and f2, f5, ··· transmit to output port B_2. This is the reason why the tripler can be built up with DCL networks. However in the case of Fig. 6 (b), the output pulses overlap each other at both edges as pointed out in Fig. 2 (c) in [2]. Referring to Fig. 5 (c) again, higher frequencies than f5 can be neglected. Therefore, in other words, it can be said that most of the waveform shown in Fig. 7 (c) comes from the transmitted component f2. The duration of an input pulse being shortened, the frequency domain spectra spread to higher bands, so that separated output pulses can be generated three times as fast as the input.

4. Simulations of Output Responses

In this section, the waveforms of output simulations will be compared with photographs in Fig. 7.

In general, when inputs and outputs are denoted by $a_T(t)$ and $b_T(t)$ in the time domain, their Fourier transforms $A_T(\omega)$ and $B_T(\omega)$ are related by

$$B_T(\omega) = \Gamma_n(\omega)\, A_T(\omega), \tag{15}$$

where $\Gamma_n(\omega)$ is the transfer function of n-section DCL network.

When $B_{1T}(\omega)$ and $B_{2T}(\omega)$ respectively represent the output Fourier transforms for the train of unipolar input pulses $a_T(t) = v_{Tr}(t)$ and for that of bipolar input pulses $a_T(t) = w_{Tr}(t)$, eqs. (16) and (17) are obtained from (11b), (13b) and (15).

$$B_{1T}(\omega) = \omega^+ \sum_{k=-\infty}^{\infty} \Gamma_n(k\omega^+)\, V(k\omega^+)\, \delta(\omega - k\omega^+), \tag{16}$$

$$B_{2T}(\omega) = \omega^+ \sum_{k=-\infty}^{\infty} \Gamma_n\{(2k+1)\omega^+/2\}\, V\{(2k+1)\omega^+/2\} \cdot \delta\{\omega - (2k+1)\omega^+/2\}. \tag{17}$$

A. Output Waveforms of Test Circuit A

When the output of P. G. in Fig. 3 (a) is assumed to be the pulse train of Fig.6 (a), we substitute $\omega^+ = \omega_1^+ = 2\pi / T_1$ and $n = 1$ into (16), where $T_1 = 5.2$nsec. Then we have the output Fourier transform of test circuit A.

$$B_{1T}(\omega) = \omega_1^+ \sum_{k=-\infty}^{\infty} \Gamma_1(k\omega_1^+)\, V(k\omega_1^+)\, \delta(\omega - k\omega_1^+). \tag{18a}$$

Taking into account the following: (i) $\Gamma_1(0) = 0$; (ii) $\Gamma_n(\omega)$ and $V(\omega)$ are even functions ; and (iii) Phase $\theta_n(\omega)$ of $\Gamma_n(\omega)$ is a odd function, the inverse transform of (18a) can be given by

$$b_{1T}(t) = \frac{2}{T} \sum_{k=1}^{\infty} \left| \Gamma_1(k\omega_1^+) \right| V(k\omega_1^+) \cos \left\{ k\omega_1^+ t - \theta_1(k\omega_1^+) \right\}. \tag{18b}$$

The sampled data for the output simulations are shown in Table I. They are obtained from the

Table 1 Sampled Data Used in Fig. 8

Freq.[MHz]	0	192	385	577	769	962	1154	1346	1538	1731
Ampli.[dB]	∞	7.0	34.0	7.0	25.0	7.2	21.0	8.0	16.9	8.9
Phase[deg.]	x	-6.1	73.8	4.9	80.9	17.4	76.1	33.0	99.6	53.3

measurement curves at the discrete frequency components in Figs. 4 (a) (b) (c). The phase data were read out from the 3-rd LMS polynomials. Applying the sampled data to (18b), we have the resultant simulation waveform in Fig. 8.

B. Output Waveforms of Test Circuit B : - Case of Input Waveform Fig. 6 (b) -

The output of test circuit B can be obtained by substituting $\omega^+ = \omega_2^+ = 2\pi / T_2$ into (17), where $T_2 = 2.6$nsec.

In the same way as in A. IV.,

$$b_{2T}(t) = \frac{2}{T} \sum_{k=0}^{\infty} \left| \Gamma_2 \{ (2K+1)\omega_2^+ / 2 \} \right| \left| V \{ (2K+1)\omega_2^+ / 2 \} \right| \cdot \cos [(2k+1)\omega_2^+ t / 2 - \theta_2 \{ (2K+1)\omega_2^+ / 2 \}]. \tag{19}$$

Applying the sampled data from Figs. 5(a) (b) (c) to (19), the resultant simulation waveform can be obtained.

C. Output Waveforms of Test Circuit B: - Case of the Waveform in Fig. 8 being input-

As the input is given by $B_{1T}(\omega)$ in (18a), we have

$$B_{2T}(\omega) = \omega_1^+ \sum_{k=-\infty}^{\infty} \Gamma_2(k\omega_1^+)\, \Gamma_1(k\omega_2^+)\, V(k\omega_1^+)\, \delta(\omega - k\omega_1^+). \tag{20}$$

In the same way as in A. IV.,

$$b_{2T}(t) = \frac{2}{T} \sum_{k=1}^{\infty} \left| \Gamma_2(k\omega_1^+)\, \Gamma_1(k\omega_1^+) \right| V(k\omega_1^+) \cdot \cos \left\{ k\omega_1^+ t - \theta_1(k\omega_1^+) - \theta_2(k\omega_1^+) \right\}. \quad (21)$$

The amplitude and phase sampled data for test circuit B can be obtained from the measurement curves in Figs. 5(a) (b), but in this case the sampling points are taken at the discrete frequency components in Fig. 4 (c). Fig. 9 shows the result. It can be said that Figs. 8 and 9 well approximate the photographs in Fig.7.

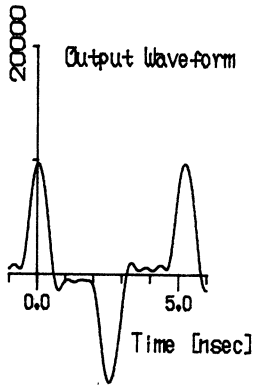

Fig. 8 The simulation of test circuit A when Fig. 6 (a) is the input.

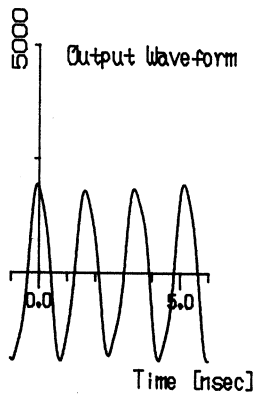

Fig. 9 The simulation of test circuit B when Fig. 8 is the input.

D. Output Responses of Ideal Networks

Using the same programs as in A., B., and C., we can show ideal output reponses. Followings are the data used here for the test circuit A.

$$\begin{cases} 6.95\text{dB and } 0^\circ & \text{at } (2k-1)\,\omega_1^+ \\ 100.0\text{dB and } 90^\circ & \text{at } 2k\,\omega_1^+ \end{cases}$$

Fig. 10 shows the output waveform using the data of $\omega_1^+ \sim 9\omega_1^+$. The frequency band of this case is 0～1731 MHz, and 99.8% of the energy of the input pulses is covered.

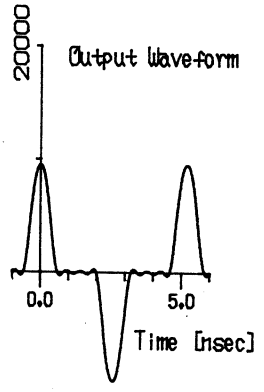

Fig. 10 A theoretical response by an ideal coupler of K = 6.95dB.

E. Output Waveforms:- Case of duration 0.66nsec-

As ststed in D. Ⅲ., when the duration of input pulses is 1.1nsec, overlaps occur at both edges of each output pulse of the test circuit B. Here let us take up the case of input pulses being shortened to 0.66nsec.

When input waveform Fig.6 (a) is applied to port A_1 in Fig. 3, the approximate output waveform of test circuit B via test circuit A is given in Flg. 11 (a). The calculation is based on (21) and measurement sampling data obtained at A. and C. in IV.. Therefore, the frequency band under

consideration corresponds to 0 ~ 1731 MHz and 99.1% of the energy of input pulses is considered here.

The ideal output response which we can expect is shown in Fig. 11 (b), where the input pulses Fig. 6 (b) are applied to port B_1. The used data at $(2k + 1)\omega_2^+/2$ are (i) 5.4 dB and 0° for k = 1, 4, 7 and (ii) 100 dB and 61.945° for k = 0, 2, 3, 5, 6. The frequency band is 0 ~ 2.885 GHz, and 99.8% of the energy of input pulses is taken into acount.

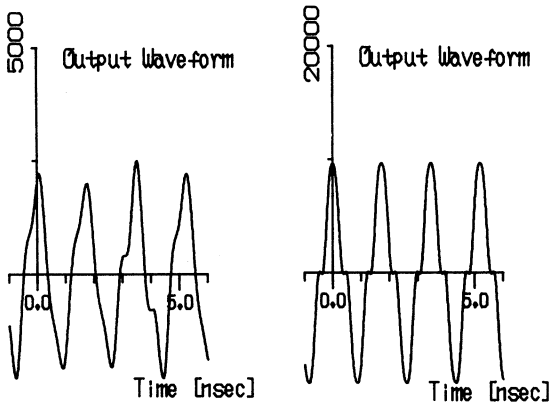

Fig. 11 Output waveforms for CHW pulses of duration τ_1 = 0.66nsec.
(a) An approximation of the output from test circuit A to B by the measured sampling data, where Fig. 6 (a) is the input.
(b) A theoretical response of an ideal 2-section network for the input Fig. 6 (b).

5. Conclusions

In Ⅱ., a cosine half wave (CHW) pulse sliced at a positive voltage level has been considered on the Fourier transform and nhe energy ratio. It has been shown no practical differences exist on the energy concentration in the frequency domain between the case of a = 1.0 and 0.5. Fig. 2 can be used to know the energy concentration on the frequency axis for the CHW pulses and rectangular pulses of arbitrary duration τ_1, since the energy ratio E_{ra} is represented as a function of $X = \tau_1\Omega$.

In Ⅲ., the energy spectra have been considered on a train of unipolar pulses and on a train of bipolar pulses. It has been found that (i) the frequency components of these periodical pulses are discrete and the amplitudes are determined by the Fourier transform of each constituent pulse, (ii) the proposed distributed coupled-line (DCL) multipliers function like passive linear filters which eliminate certain frequency components and pass others that the trains of input pulses originally possess, and (iii) although the network transfer functions are obtained on the basis of TEM wave approximations, the fabricated DCL networks (test circuits A and B) have satisfied the prescribed frequency characteristics in the frequency band where almost all the input energy concentrates.

In IV., the output simulations of the fabricated DCL networks have been obtained from a few

sampling measurement data by using a 16 bit personal computer and MS-FORTRAN 77. The results have shown good agreements with the experimental photographs.

The experimental networks, test circuits A and B, are handmade, using copper clad laminates. Therefore, precise fabrications with low loss materials will provide even better output waveforms for the input pulse of shorter duration.

Acknowledgment

The author is grateful to professor K. Hatori and to three undergraduate students of Hokkaido Institute of Technology for their cooperation in measuring phase characteristics.

Appendix [4]

The Definitions of the Effective Duration Δt and Effective Bandwidth $\Delta \omega$

Under the condition of $\int_{-\infty}^{\infty} t \,|\, v\,(t) \,|^{\,2}\, dt = 0$,

$$(\Delta t)^2 = \int_{-\infty}^{\infty} t^2 \,|\, v\,(t) \,|^{\,2}\, dt, \tag{A. 1}$$

$$(\Delta \omega)^2 = \int_{-\infty}^{\infty} \omega^2 \,|\, v\,(\omega) \,|^{\,2}\, d\omega, \tag{A. 2}$$

where $V\,(\omega)$ is the Fourier transform of v (t).

Theorem

On the effective bandwidth $\Delta \omega$ of a duration-limited pulse waveform v (t),

$$\Delta \omega \geq \pi \,/\, (\tau_1) \tag{A. 3}$$

where τ_1 is the duration.

Equality is only achieved when

$$v\,(t) = \begin{cases} \sqrt{\dfrac{2}{\tau_1}} \cos\left(\dfrac{\pi}{\tau_1} t\right), & |\, t \,| \leq \tau_1 / 2 \\ 0 \quad , & |\, t \,| > \tau_1 / 2 \end{cases} \tag{A. 4}$$

The Energy Ratio of a Rectangular Wave

When a rectangular wave is represented by

$$v(t) = \begin{cases} A, & |t| \leq \tau_1 / 2 \\ 0, & |t| > \tau_1 / 2 \end{cases}$$

the energy ratio within $|\omega| \leq \Omega$ is defined by

$$E_{ra} = \int_{-\Omega}^{\Omega} |v(\omega)|^2 \, d\omega \Big/ \int_{-\infty}^{\infty} |v(\omega)|^2 \, d\omega, \qquad \text{(A. 5)}$$

where $V(\omega) = \tau_1 \, \mathrm{Asin}(X/2)/(X/2)$ and $X = \omega \tau_1$.

References

[1] I. Sakagami, N. Miki, N. Nagai, and K. Hatori, "Digital frequency multipliers using multi-section two-strip coupled line," IEEE Trans. Microwave Theory Tech., vol. MTT-29, pp. 118-122, Feb. 1981.

[2] I. Sakagami, N. Nagai, and K. Hatori, "On Reducing the Period of Input Pulse Trains Using Coupled-Line Networks," IEEE Trans. Microwave Theory Tech., vol. MTT-35, pp. 409-414, April 1987.

[3] B. P. Lathi, Communication Systems. New York: Wiley, 1977, ch. 1.

[4] T. Hosono, Fundamentals of Information Engineering. Corona Publishing, 1970. (in Japanese)